Check for updates

Received: 28 March 2022 | Revised: 11 July 2022 | Accepted: 22 July 2022

DOI: 10.1002/aoc.6837

RESEARCH ARTICLE

Applied Organometallic Chemistry WILEY

Pyridine-functionalized N-heterocyclic carbene gold(I) binuclear complexes as molecular electrocatalysts for oxygen evolution reactions

Zhoveta Yhobu[1] | **Geetha Basappa Markandeya**[1] | **Jan Grzegorz Małecki**[2] | **Hosapalya Thimmaiah Srinivasa**[3] | **Rangappa S. Keri**[1] | **Doddahalli Hanumantharayudu Nagaraju**[4] | **Mohammad Azam**[5] | **Saud I. Al-Resayes**[5] | **Srinivasa Budagumpi**[1]

[1]Centre for Nano and Material Sciences, Jain University, Jain Global Campus, Bangalore, India

[2]Institute of Chemistry, University of Silesia, Katowice, Poland

[3]Soft Condensed Matter Group, Raman Research Institute, Bengaluru, India

[4]Department of Chemistry, School of Applied Sciences, REVA University, Bangalore, India

[5]Department of Chemistry, College of Science, King Saud University, Riyadh, Saudi Arabia

Correspondence
Srinivasa Budagumpi, Centre for Nano and Material Sciences, Jain University, Jain Global Campus, Kanakapura, Ramanagaram, Bangalore 562112, India.
Email: b.srinivasa@jainuniversity.ac.in

D. H. Nagaraju, Department of Chemistry, School of Applied Sciences, REVA University, Kattigenahalli, Yelahanka, Bangalore 560064, India.
Email: dhnagu@gmail.com

Funding information
King Saud University, Grant/Award Number: RSP-2021/147; Department of Science and Technology, New Delhi, India, Grant/Award Number: DST/TDT/DDP-33/2018

N-heterocyclic carbene (NHC) complexes of gold(I/III) attained immense interest in catalytic organic transformations and as anticancer agents against several types of human cancers; however, their potential as electrocatalysts is scarce. The electrocatalytic oxygen evolution reaction was performed for the first time using pyridine-functionalized NHC gold(I) binuclear metallacycles (**8** and **9**) possessing aptly designed ligand field. Complexes were prepared by the transmetallation of corresponding silver(I) NHC complexes, which were prepared by in situ deprotonation of pyridine and aryl substituted 1,2,4-triazolium hexafluorophosphate salts (**6** and **7**) with Ag_2O under dark. Both triazolium salts and binuclear gold(I) metallacycles were thoroughly characterised by NMR and ATR-IR spectral and elemental analyses. A bromide salt **4** and a binuclear gold complex **9** were elucidated for structure by single crystal X-ray diffraction analysis. Complex **9** possesses distorted linear coordination geometry around the gold atoms by the coordination of carbene carbon and pyridine nitrogen atoms bearing close Au–Au interaction (3.251 Å). The binuclear gold complexes **8** and **9** (along with 10 wt% conductive mesoporous carbon) were investigated as molecular electrocatalysts in oxygen evolution reaction (OER), which evidenced an oxygen evolution overpotential of 2.422 and 2.370 V versus reversible hydrogen electrode (RHE), respectively, to attain a current density of 10 $mA.cm^{-2}$. The Tafel slope values of 40.9 and 30.4 mV dec^{-1} for **8** and **9**, respectively, indicate the reaction mechanism involved and the suitability of these complexes as apt electrocatalysts for OER. The stability of the prepared molecular electrocatalysts was investigated by cyclic voltammetry and chronoamperometry techniques.

KEYWORDS
1,2,4-triazoles, molecular electrocatalyst, N-heterocyclic carbene, oxygen evolution reaction, X-ray diffraction

 © 2022 John Wiley & Sons, Ltd.

1 | INTRODUCTION

The first venture to isolate and synthesise organogold compounds began in 1864 by treatment of alkyl mercury compounds with metallic gold, but it was found unsuccessful due to the amalgamation of both the metals.[1] Their existence only came to be much later in 1907, when Pope and Gibson were able to isolate diethylgold(III) bromide.[2] This was followed by isolation of the first trialkyl gold complex in 1948[3] and the introduction of phosphine ligands followed much later, in 1963.[4] The field of organogold chemistry has come a long way since then; it has found importance in various applications ranging from heterogeneous and homogeneous catalysis[5–10] to medicinal chemistry.[11] It may be noted that the various and tremendous work employing organogold as catalysts is predominant to gold(I) and gold(III) compounds that possess "ligandless" systems like gold(I) and gold(III) chloride salts and the rare usage of phosphine containing species.[8,12–14]

On the other hand, stable N-heterocyclic carbenes (NHCs) that were first isolated by Arduengo in 1991[15] have considerably gained popularity over the years and have become a proven choice as an imperative class of ligands in organometallic chemistry. NHCs as ligands feature strong stabilising effects because of the π-donating substituents that warrants for the strong σ-electron sharing properties, which also allows for strong carbene carbon−metal bond.[16] Their inherent ability to stabilise active metal atoms in varying oxidation states has also made it an important choice of ligands. In organogold chemistry, gold(I) and gold(III) species have been extensively explored, and of these two, gold(I) has garnered a lot of interest and has been used in various applications.[17] The results of these developments have enabled for spectroscopic and structural aspects of gold(I)–NHC complexes to be widely explored; however, the electrochemistry aspects of these complexes are still relatively less.[18,19] The application of gold(I)–NHC complexes as electrocatalysts are relatively lesser; one of the first reports was the development of gold(I)–NHC complexes as an electrochemical sensors for the detection of glucose.[17] Recently, we have reported the employment of gold(I)–NHC complexes as electrocatalysts for hydrogen evolution reaction (HER).[20] In this paper, we report another interesting fact of using NHC complexes to explore electrocatalytic applications, that is, pyridine-functionalized NHC gold(I) binuclear complexes as electrocatalysts for the oxygen evolution reaction (OER), to evaluate their standings as OER catalysts and their potential in the field of electrocatalysis. For electrocatalytic OER, high-valence late transition metal-based catalysts gained enormous attention, which could be attributed to the feasible interaction of these metal species with OER intermediates. Alongside, the selection of an appropriate corrosion-resistant support material that provides required robustness to the active electrocatalysts for the OER is an important task. For which, frequently employed conductive carbon material are nanotubes and carbon black; however, at high applied potentials, these suffer from drop in stability.

The major advantages of using molecular electrocatalysts for OER are being (i) the catalyst loading is quantifiable, (ii) catalyst material formed on the electrode surface is through self-assembly of the molecules as the complex solution is used for electrode modification unlike suspensions in the case of metal nanoparticles, and (iii) low metal content.[21] Presumably, the usage of the catalysts may address the apt designs for OER electrocatalysts, which in turn helps provide solution for the pressures of energy shortage, the gradual decline in carbon-based fuels, and the pollution of the environment. This has directed and influenced human civilisation to take a call for greener energy sources and a cleaner environment. The development of efficient energy conversion devices in this aspect becomes crucial in solving this crisis.[22,23] OER catalysis in this regard plays an important role in the overall water splitting to yield hydrogen gas; OER involves a four-electron process and the kinetics of which is sluggish, and as such, this is the rate determining step in the water splitting process.[24–26] The commercial catalysts of OER are very expensive, and as such, tremendous amount of research has been carried out to develop catalysts that is inexpensive, efficient, and green.[27,28] In this work, we have developed electrocatalysts from binuclear gold(I) complexes bearing pyridyl and aryl substituted 1,2,4-triazoles. The gold(I) complexes were investigated as OER electrocatalysts in basic media in a conventional three electrode set-up.

2 | RESULTS AND DISCUSSION

Gold(I)–NHC complexes have been explored in various capacities and have shown excellent results especially in the field of anticancer and antimicrobial applications. In the field of electrochemistry, there still seems to be a lot of gaps that needs to be covered. The electrochemical investigations of gold(I)–NHC complexes have been reported over the years[18,19]; however, employing these complexes in an electrochemical application is limited and rare. We have recently reported a series of complexes as electrocatalysts for HER, wherein the effectiveness of these complexes in electrochemical hydrogen evolution has been examined. The possibilities and scope of gold(I)–NHC complexes have yet to be fully ascertained,

particularly while using these complexes as heterogeneous electrocatalysts rather than the homogeneous counterparts. The homogeneous electrocatalysts with NHC-based complexes have up to an extent been explored for CO_2 and proton reduction reactions.[29–32] We believe that this work will offer new insights into gold(I)–NHC chemistry as heterogeneous electrocatalysts and their future in electrocatalysis.

2.1 | Synthesis and characterisation of pyridyl and aryl substituted 1,2,4–triazolium salts (4–7) and their binuclear gold(I) complexes (8 and 9)

In this present study, two sterically tuned bis-NHC coordinated binuclear gold(I), **8** and **9**, complexes with varied substituents were synthesised. A pyridyl ring was anchored on two different aryl substituted 1,2,4-triazole ring systems through a simple quaternization reaction.[33] The triazolium bromide salts **4** and **5** were prepared in excellent yields by the reaction of 2-(bromomethyl)pyridine hydrobromide (**1**) with 4-(2,6-diethylphenyl)-4H-1,2,4-triazole (**2**)/4-(2,4,6–trimethylphenyl)-1,2,4-triazole (**3**), respectively, in 1,4–dioxane at reflux reaction condition for 48 h. Further, these bromide salts, **4** and **5**, were treated with KPF_6 in methanol and water mixture to yield pyridyl and aryl substituted 1,2,4-triazolium hexafluorophosphate salts **6** and **7** as depicted in Scheme 1 following salt metathesis protocol.

Further, the hexafluorophosphate salts **6** and **7** were initially treated with Ag_2O in 2:1 molar ratio in acetonitrile at 45°C under dark for 24 h to afford bis-NHC coordinated binuclear silver(I) hexafluorophosphate complexes through in situ deprotonation pathway. After the stipulated time, the reaction mixture was passed through a bed of celite, and the silver complexes in acetonitrile solution were collected. To the solution of silver complexes of **6** and **7** were treated with [AuCl (SMe_2)] in acetonitrile and stirred at room temperature for 4 h in dark to yield pyridine-functionalized NHC binuclear gold(I) complexes **8** and **9**, respectively, through transmetallation reaction protocol[34] as depicted in Scheme 2.

Initially, it was thought that pyridine nitrogen atoms would involve in coordination with the gold atom that is coordinated by the same carbene carbon to provide additional stability; however, binuclear gold(I)–bis (NHC) metallacycles were resulted in good yields. The orientation of the dimer complex follows a head-to-tail trend with the methylene of pyridine as the spacer. Each gold atom is coordinated to the carbene carbon of one of the two participating ligands, the pyridine of the other ligand with an aurophilic interaction as illustrated in Scheme 2. Both the complexes are soluble in polar solvents and insoluble in non-polar ones.

The ^{1}H NMR spectra of the synthesised triazolium salts **6** and **7** in d_6-DMSO exhibited two characteristic singlet peaks observed at approx. δ 10.78 and 9.55 ppm corresponding to the resonances of C5 and C3 protons of 1,2,4-triazole, respectively.[16,35] In the case of salt **6**, a triplet and a quartet peaks appeared at δ 1.05 and 2.32 ppm corresponding to the resonances of methyl and methylene protons of phenyl substitution, respectively. The presence of the slightly downfield shifted singlet peak in the region δ 5.95 ppm is attributed to the resonance of protons of methylene module that connects the 1,2,4-triazole core with pyridine ring. The presence of peaks from between δ 7.40 and 8.49 ppm is attributed to the resonance of the aromatic protons of pyridyl and phenyl rings. A similar trend was observed in the ^{1}H NMR spectrum of the triazolium salt **7**, where the peaks at δ 2.09 and 2.32 ppm are attributed to the resonance of *ortho*- and *para*-methyl protons of the 2,4,6-trimethylphenenyl substitution. The singlet peak at δ 5.95 ppm corresponds to the resonance of N–CH_2 protons that connects the pyridyl ring to aryl 1,2,4-triazole. The aromatic protons exhibited similar resonances as that of salt **6** and similar reports.[36] The ^{1}H NMR spectra

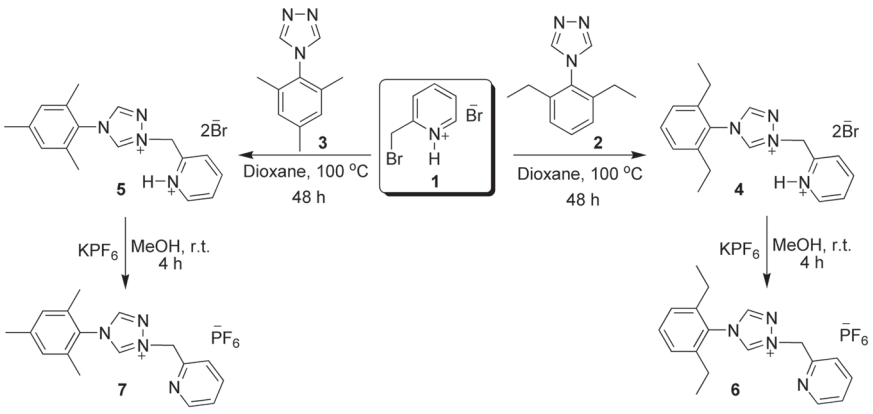

SCHEME 1 Synthesis of pyridine and aryl substituted 1,2,4-triazolium bromide salts **4** and **5** and hexafluorophosphate salts **6** and **7**

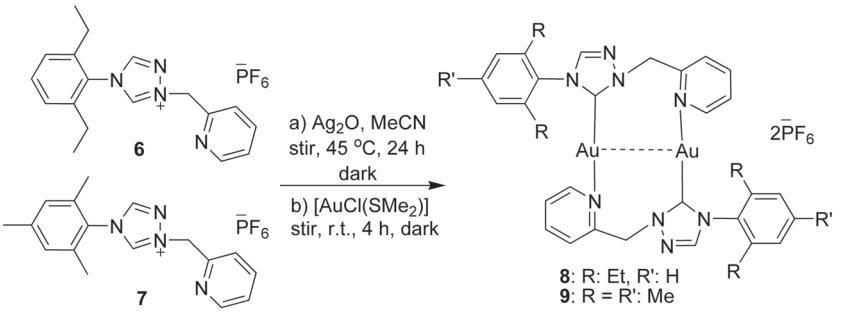

SCHEME 2 Synthesis of pyridine-functionalized NHC binuclear gold(I) metallacycles **8** and **9** via transmetallation protocol

of the pyridine-functionalized NHC binuclear gold(I) complexes **8** and **9** displayed no resonance peak at approx. δ 10.78 ppm indicating the successful deprotonation of C5 proton of the corresponding salt followed by coordination of the carbene carbon to the metal centre, which is a characteristic evidence for the formation of desired NHC coordinated complexes.[37,38] The remaining proton resonance peaks of the complexes resembled the resonance peaks observed for the corresponding salts and complex reports in the literature. There arises another coordination from the nitrogen of pyridine pendant of adjacent NHC unit to the metal centre and aurophilic interactions; these coordination's however show very little influence in the complex spectra.

In the ^{13}C NMR spectrum of salt **6** in d_6-DMSO, three distinguished carbon resonance peaks appeared at δ 11.8, 15.6, and 51.0 ppm attributed to the resonances of methyl, methylene carbon nuclei of phenyl substitution, and pyridyl methylene carbon, respectively. In the region δ 124–151 ppm, the peaks observed are ascribed to the resonances of phenyl and pyridyl aromatic carbon nuclei. A set of distinct aromatic peaks appeared at δ 145.9 and 146.2 ppm corresponding to the resonances of C3 and C5 carbon nuclei of triazole, respectively. Similarly, the ^{13}C NMR spectrum of **7** in d_6-DMSO exhibited three distinguished carbons resonance peaks at δ 17.6, 21.1 and 56.5 ppm attributed to the resonances of *ortho*- and *para*-methyl and pyridyl methylene carbon nuclei, respectively. The aromatic carbon resonance peaks were similar to that of salt **6** including aromatic peaks at δ 145.5 and 145.9 ppm correspond to the resonances of C3 and C5 carbon nuclei of triazole, respectively.

The ^{13}C NMR spectrum of binuclear gold(I) complex **8** bearing pyridyl-functionalized NHC ligand displayed a carbon resonance peak at δ 186.8 ppm, corresponding to the resonance of carbene carbon atom bound to the gold atom.[16,38] This huge downfield shift of C5 carbon of 1,2,4-triazole core indicates the successful formation of pyridine-functionalized NHC binuclear gold(I) complexes. Similarly, in the ^{13}C NMR spectrum of binuclear gold(I) complex **9**, the resonance peak at δ 168.8 ppm is attributed to C5 carbon of 1,2,4-triazole. This downfield of the C5 triazole when compared with the salt spectrum evidences the successful deprotonation of the proton at C5 followed by coordination to the gold atom.[39] The peaks corresponding to the aliphatic and aromatic carbons resembled the spectra of the salts. It may be noted that the complexes **8** and **9** exhibit counter peaks for the resonance of carbon nuclei, which is a common behaviour in a complex that exhibit rotamerism.[20,40]

Congruently, ATR-IR spectra of the salts and binuclear gold(I) complexes were recorded over 500–3600 cm^{-1} range. The salts and complexes displayed distinct strong band with high intensity at ~2900, 1615, and 1019 cm^{-1} attributed to the stretching vibrations of C–H, C=N, and C=C/C–N module of pyridine/triazole, respectively,[41] which were found almost unaffected in the complex spectra except the C=N stretching bands. The C=N/C–N module of pyridine shows a slight shift to higher wavenumber, which undoubtedly confirms the involvement of pyridine heterocyclic nitrogen atom in coordination with the gold atom.

2.2 | Single crystal XRD analysis

The molecular structure of a triazolium salt bearing a bromide counterion (**4**) and a binuclear gold complex (**9**) was elucidated by single crystal X-ray diffraction method. The single crystals of salt suitable for analysis were grown from slow evaporation of its methanolic solution over a period of 7 days, while complex crystals were collected from slow diffusion of diethyl ether into dichloromethane–acetonitrile (1:1 v/v) solution of the complex at room temperature. The structure refinement and crystallographic data for **4** and **9** are tabulated in Table S1. The bond distances and bond angles of the salt are provided in Tables S2 and S3, respectively. The salt **4** (Figure 1a) crystallised in the monoclinic crystal system with a space group $P2_1/c$ having two bromide anions, a triazolium cation, and a co-crystallised water molecule in an asymmetric unit. In the triazolium core, the internal ring angles at C3 and C5 carbons N3–C1–N1 and N3–C2–N2 were 107.5(3) and 111.8(3)°, respectively. The

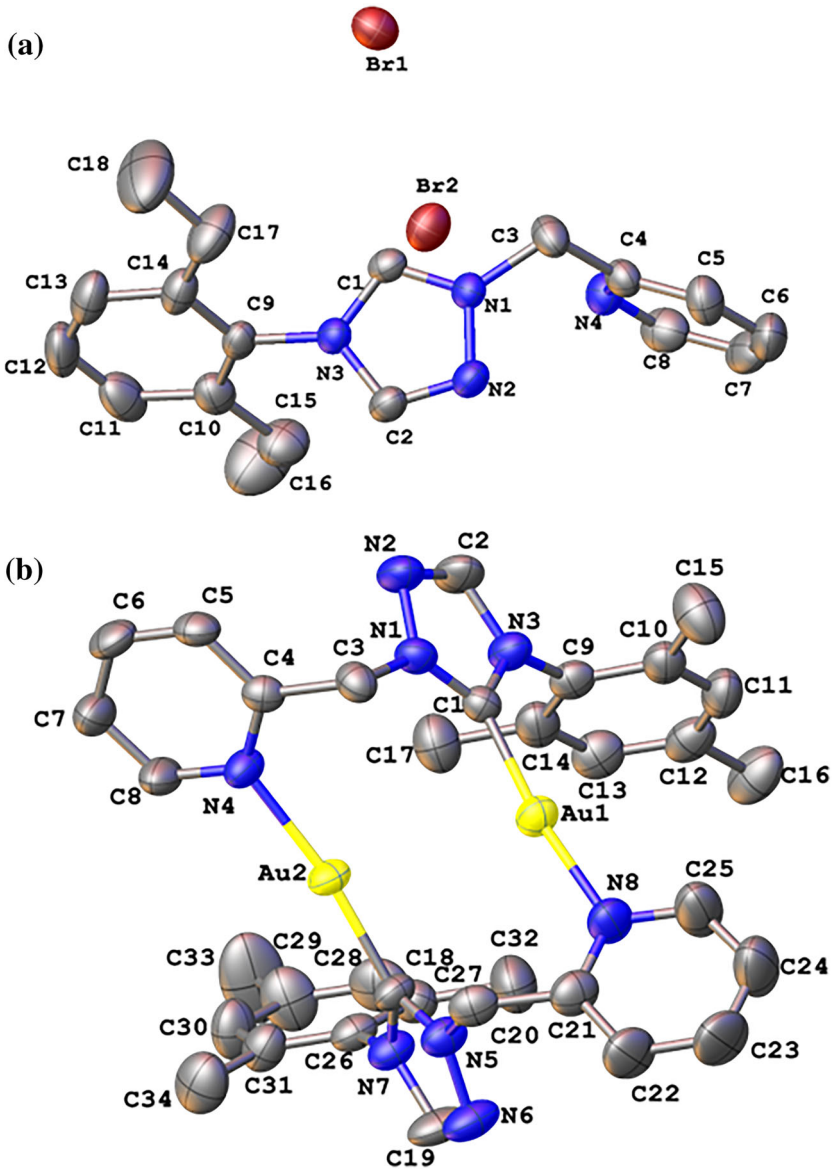

FIGURE 1 Crystal structure of 1,2,4-triazolium salt **4** bearing pyridyl and 2,6-diethylphenyl substitutions (a) and binuclear gold(I) metallacycle **9** (b). Hydrogen atoms, hexafluorophosphate anions, and co-crystallised water molecule are excluded for clarity. The ellipsoids are drawn with 30% probability levels.

methylene arm that tethered the triazole to the pyridyl ring (C4–C3–N1) was at an angle of 111.1(3)°. The observed bond distances were all in the range of 1.294 (5)–1.508(5). The bond distances and bond angles of the molecules were found to be in agreement with the analogous salts that have been reported earlier.[16] Surprisingly, the pyridine nitrogen atom is protonated to form pyridinium appendant whose charge is counterbalanced by a bromide anion. It is evident from the X-ray analysis that this structure is precipitated in the form of 1:2 electrolyte, with two counter bromide anions and a triazolium cation. In the comprehensive structure of the salt, two different π–π stacking interactions are found between pyridine-phenyl and phenyl-pyridine rings of adjacent molecules (Figure 2a) with a centroid-centroid distance of 3.862 and 3.885 Å bearing a shift distance of 1.112 and 1.475 Å, respectively. Alongside, several types of hydrogen bonding interactions found operating between bromide counterions and C–H modules of triazolium cation with the interaction distance in the range 2.224–2.926 Å in the crystal diagram (Figure 2b) along with several hanging contacts.

The molecular structure of the dimeric, pyridine-functionalized NHC binuclear gold(I) complex **9** bearing hexafluorophosphate counterions is depicted in Figure 1b, and the important bond distances and angles are tabulated in Tables S4 and S5, respectively. Complex **9** crystalized in the monoclinic crystal system with a $P2_1/c$ space group bearing two hexafluorophosphate counterions and a complex cation in a unit cell. The introduction of gold cations into the NHC system results in the formation of a pyridine-functionalized NHC binuclear gold(I) complex. The complex consists of two gold atoms each bridged to a NHC donor and a

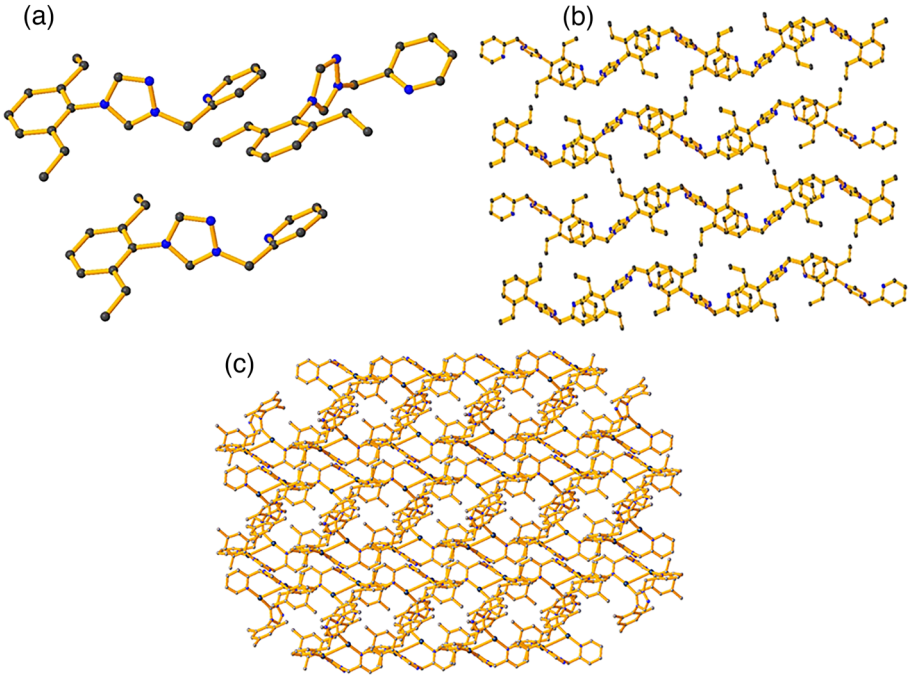

FIGURE 2 Molecular stacking (a) and packing (b) diagrams of triazolium bromide salt **4** and packing diagram (c) of complex **9**. Counter bromide/hexafluorophosphate anions, hydrogen atoms, and co-crystallised water molecule are excluded for clarity.

pyridine nitrogen in a "head-to-tail" arrangement.[41] The ligand supported aurophilic interaction, that is, Au1–Au2 was found to have a bond distance of 3.250 (4) Å, which is slightly higher than the distance between two gold atoms in the elemental gold (2.88 Å), while is in well agreement with the similar interaction found in the literature.[40] The Au1–C1 (1.964(6) Å) and Au2–C18 (1.971(6) Å) bond distances are almost the same, and similarly, Au1–N8 (2.063(6) Å) and Au2–N4 (2.070(5) Å) are also comparable with each other. Both the gold atoms possess distorted linear coordination geometry by the involvement of carbene carbon and the pyridine nitrogen atoms with the bond angle 170.8(2)° for C1–Au1–N8 and 171.6(2)° for N4–Au2–C18. This deviation from linearity is probably due to the strong interactions operating between gold atoms and the fluorine atoms of hexafluorophosphate counterions (Au1–F10: 3.251 Å and Au2–F2: 4.813 Å) along with aurophilic interactions. Alongside, the internal bond angle at carbene carbon atom found to be 103.4 (5)° for N3–C1–N1 and 103.0(5)° for N5–C18–N7, which are in well agreement with the earlier similar reports.[40] The differences in the bond distances and angles of both the NHC units may be attributed to the twisting of the methylene bridge between the triazole core and the pyridine pendant. In the crystal packing of the complex, several types of hydrogen bonding interactions are found operating between hexafluorophosphate counterions and binuclear gold complex cations in the range 2.225–2.917 Å as shown in Figure 2c.

2.3 | Morphological studies of pyridine-functionalized NHC binuclear gold(I) complexes

Understanding the morphology of the thin film that is drop-casted on the surface of the glassy carbon electrode (GCE) is crucial in attaining the intrinsic electrocatalytic activity. In this regard, we have investigated the morphology of both the binuclear gold metallacycle complexes by field emission scanning electron microscope (FE-SEM). The gold complexes were dissolved in dichloromethane (0.003 M) by sonication for about 10 min, and 3 μl aliquot complex solutions were drop-casted on a silicon wafer. The stark difference in the morphology despite the complexes bearing identical molecular structure is attributed to the difference in alkyl arms on the phenyl ring of complexes. The uneven, irregular, and rough morphology on complex **8** in Figure 3a is presumably due to the longer alkyl arms on the phenyl ring, which may result in hindering the supramolecular assembly of the complex cations and anions. This affects the film formation resulting in uneven, improper orientation and inefficient distribution and exposure of the active sites during the electrochemical OER process. Complex **9** bears comparatively shorter alkyl arms on the phenyl ring and as a result exhibits well-defined grain boundaries and distinct morphology shown in Figure 3b, which presumably results in better and more efficient exposure of its active sites for electrochemical adsorption of intermediate oxygen species which ensues in the formation and evolution of oxygen gas.

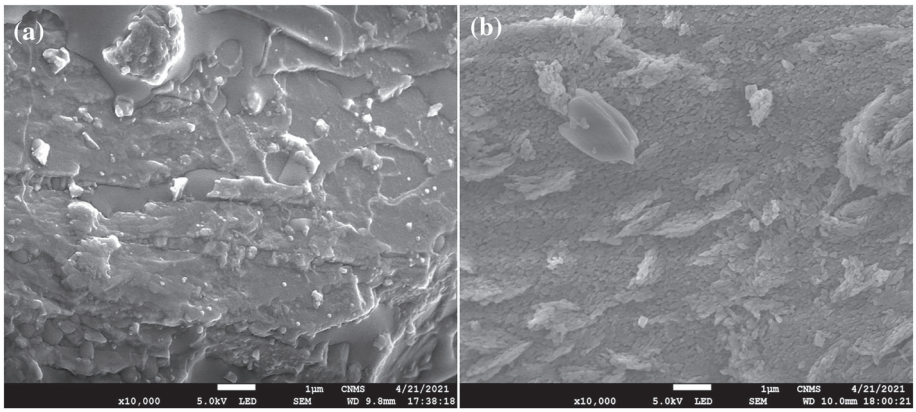

FIGURE 3 FE-SEM images of the films formed by the evaporation of dichloromethane solution of binuclear gold metallacycles **8** (a) and **9** (b)

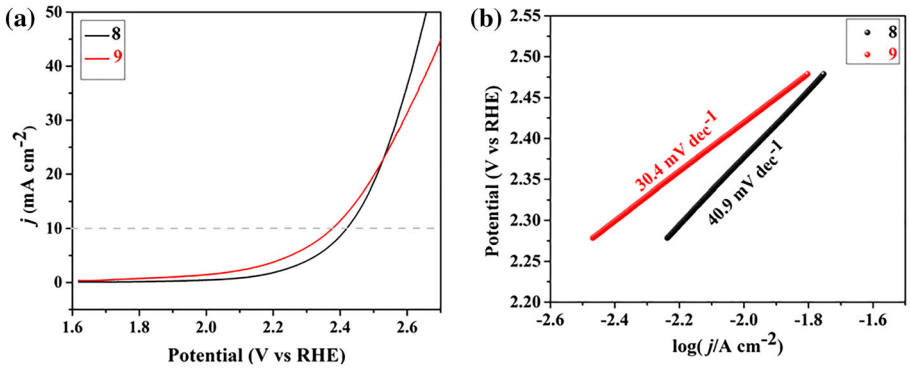

FIGURE 4 (a) LSV for complexes **8** and **9** at a scan rate of 5 mV s^{-1} in 1 M KOH. (b) Tafel plots of complexes **8** and **9** calculated from LSV curves

2.4 | Electrocatalytic oxygen evolution activity and stability studies

Design and development of promising OER electrocatalysts that can be performed in neutral electrolytes such as untreated water is highly difficult and interesting due to their low conductivities and relatively slow OER kinetics. Electrocatalysts for OER may suffer from lack of conductivity and corrosion or leaching of the catalyst from the electrode surface, and hence to make them corrosion resistant and to increase the conductivity, the carbon support materials such as carbon blacks, reduced graphene oxide, carbon nanoribbons, or carbon nanotubes have been used. In this context, in the present work, we have used graphitic mesoporous carbon black as conductive material that also provides corrosion resistance property to the electrocatalysts. To a suspension of 0.003 M gold(I) metallacycles (**8** or **9**) solution in dichloromethane was added 10 wt% of graphitic mesoporous carbon black and sonicated to prepare a suspension, of which 3 μl was used to drop-cast the electrodes. The gold complex/carbon modified working electrodes were investigated for electrochemical oxygen evolution performance in an alkaline medium, that is, 1 M KOH solution. The OER activity was measured using linear sweep voltammetry (LSV) technique at a scan rate of 5 mV s^{-1}. All potentials were documented by using Standard Calomel Electrode (SCE) (3.5 M KCl) as reference electrode, and later converted to reversible hydrogen electrode (RHE) with appropriate conversion factor.

The OER performance of complexes **8** and **9** with mesoporous carbon is shown in Figure 4a. The complex **8** modified glassy carbon electrode displayed an on-set potential of 2.02 V versus RHE and a relatively high overpotential of 1.192 V versus RHE to achieve the bench mark current density of 10 mA cm^{-2}. However, the complex **9** modified electrode evidenced slightly improved OER activity with an on-set potential of 1.75 V versus RHE bearing an overpotential of 1.140 V versus RHE to acquire the same current density of 10 mA cm^{-2}, which is an important parameter for the consideration of the development water splitting device.[42] The difference in the on-set and overpotentials obtained for both the binuclear gold complexes are presumably attributed to the different alkyl substituents present on phenyl rings of NHC ligands. Alongside, in the case of complex **9**, the increased activity may probably due to the evenly distributed nanogranular structures over the electrode surface that might adsorb more OH ions or water molecules, which in turn react with metal atoms and eventually produces O_2 species. The trend in oxygen evolution is similar to that of bulk gold and gold electrodes.[43,44]

The Tafel slope, an important parameter for determining the reaction kinetics, was calculated from LSV

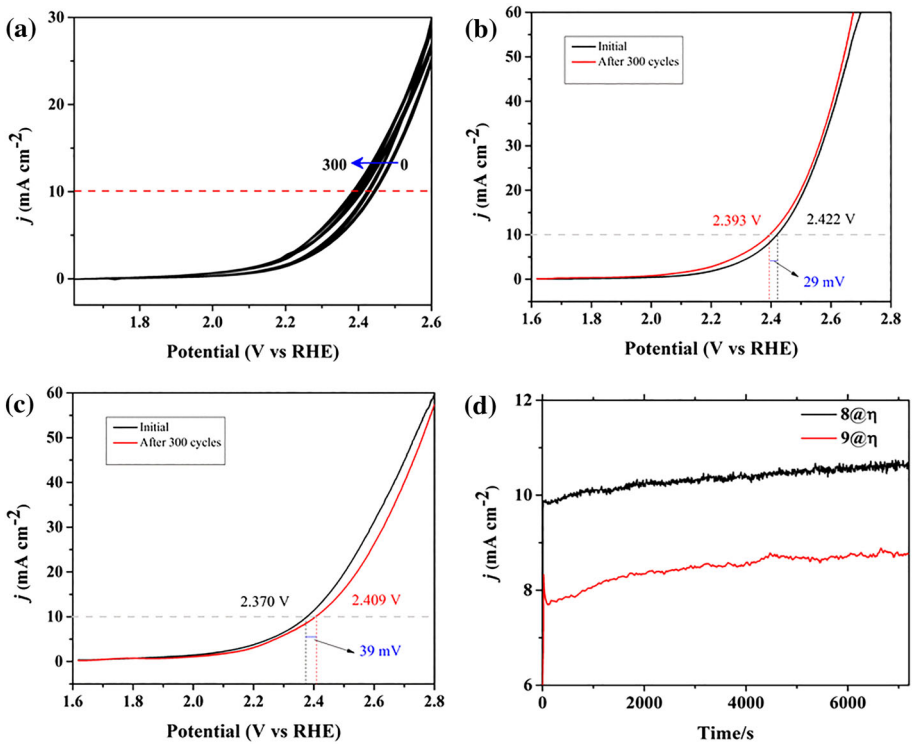

FIGURE 5 (a) Cyclic voltammograms of complex **8** displaying cyclic stability for 300 cycles in 1 M KOH at a scan rate of 5 mV s^{-1}. (b) LSV of complex **8** before cyclic stability and after cycling for 300 cycles in 1 M KOH at a scan rate of 5 mV s^{-1}. (c) LSV of complex **9** before cyclic stability and after cycling for 300 cycles in 1 M KOH at a scan rate of 5 mV s^{-1}. (d) Chronoamperometric stability test of complexes **8** and **9** at their respective overpotential of in 1 M KOH

polarisation curves of complexes using the Tafel equation given in Equation 1.

$$\eta = b \log\left(\frac{j}{jo}\right) \tag{1}$$

where η is the overpotential; b, j, and jo denote the Tafel slope, current density, and exchange current density, respectively. The Tafel plots are shown in the Figure 4b that are derived from Figure 4a for both the gold complexes. Complexes **8** and **9** possess Tafel slope value of 40.9 and 30.4 mV dec^{-1}, respectively. A lower Tafel slope value in the case of complex **9** modified electrode reflects the better electrocatalytic activity and the overpotential. From the Tafel slopes, the mechanism for OER in alkaline media can be expressed with the Equations 2, 3, 4, and 5. By virtue of the Tafel slope values, the rate determining step of OER in these cases is attributed to the Equation 5.[27,45–47] Here, M is the metal active surface site.

$$M + OH^- \rightarrow MOH + e^- \tag{2}$$

$$MOH + OH^- \rightarrow MO^- + H_2O \tag{3}$$

$$MO^- \rightarrow MO + e^- \tag{4}$$

$$2MO \rightarrow 2M + O_2 \tag{5}$$

The electrochemical cyclic stability of the electrocatalysts **8** and **9** was investigated by performing the cyclic voltammetry in the potential range 1.6 to 2.8 V versus RHE for 300 cycles (Figure 5a for complex **8**). Figure 5b,c shows the LSVs obtained by the electrocatalysts **8** and **9** modified glassy carbon electrodes before and after cyclic stability for 300 cycles at a scan rate of 5 mV s^{-1}. Complex **9** showed minimal loss in its efficiency after 300 CV cycles; the overpotential shifted from 2.370 to 2.409 V versus RHE with a potential shift of ~39 mV versus RHE as shown in Figure 5c. Conversely, complex **8** displayed increased efficiency with subsequent cycling, the overpotential to achieve a current of 10 mA cm^{-2} decreased from 2.422 to 2.393 V versus RHE indicating a shift of ~29 mV versus RHE. The change in the efficiency was further investigated by chronoamperometric technique at the individual overpotentials of the two electrocatalysts, and the results are shown in Figure 5d. The chronoamperometric test of complex **8** at a fixed potential of 2.422 V versus RHE displayed a current density of 9.8 mA cm^{-2} initially, but with the increased duration, there was an increase in the current density and at 7200 s (2 h) the current density was 10.6 mA cm^{-2}, this result is in agreement with polarisation curve depicted in Figure 4a, wherein with subsequent cycling the overpotential has been decreased. The complex **9** showed similar characteristic in the cyclic stability studies, the

chronoamperometric test at a fixed potential of 2.370 V versus RHE exhibited a current density of ~7.7 mA cm^{-2} initially, and the current density, however, started to increase with the increase in duration. The current density at the end of the stability test had increased to ~8.7 mA cm^{-2}, but it was unable to reach the benchmark current density. The chronoamperometric studies of complex **8** after 2 h demonstrated increased electrocatalytic potential which could be presumably due to the reorientation of complex molecules on the electrode surface in such a way that more metal atoms can interact with the OER intermediates.

OER electrocatalysis by sterically varied gold complexes **8** and **9** can be concluded that the superior performance of the latter catalyst in terms of on-set and overpotential compared with the former catalyst is attributed to the change in the steric environment around the gold atom, while the increased stability of complex **8** after 2 h is ascribed to the reorientation of the catalyst molecules on the electrode surface.

The electrochemical OER overpotential displayed by the two electrocatalysts (i.e., **8** = 1192 mV and **9** = 1140 mV vs. RHE) compared with commercial OER catalyst like Ru/C@390 mV versus RHE and Ir/C@380 mV versus RHE are indicative that the developed electrocatalysts requires a lot of tuning and further investigation.[48] Other than the commercial catalysts, there have been efforts in developing catalysts for OER from materials like Au-nano particles,[44] covalent organic frameworks,[49] transition metal oxides/chalcogenides,[27] and so forth. It may be noted that this work like many others is also aimed at developing efficient, environmentally benign, abundant, economical electrocatalysts for OER. While other materials have been already established and developed as potential OER catalysts, this is the first work highlighting the possibilities of employing NHC complexes as OER electrocatalysts, and there is still lots of improvement and combinations that can be explored for efficient NHC-based OER electrocatalysts.

3 | CONCLUSIONS

Two pyridine-functionalized NHC binuclear gold(I) metallacycles **8** and **9** have been prepared and employed as electrocatalysts for OER in an alkaline medium. The complexes were prepared following the transmetallation protocols using corresponding binuclear silver(I) NHC complexes, which were prepared in situ from the NHC precursor salts through deprotonation pathway. Both sterically varied salts and binuclear gold(I) complexes were characterised by various spectral and analytical techniques. These complexes are the first gold NHC examples that have been studied for heterogeneous OER electrocatalysis. The complexes with graphitic mesoporous carbon composites were employed in the OER electrocatalysis, which displayed slightly higher overpotentials, that is, 1.192 and 1.140 V versus RHE for complexes **8** and **9**, respectively. The evaluation of these complexes for OER indicated good electrochemical stability from the cyclic voltametric and chronoamperometric tests. The Tafel slope values are indicative of mechanisms that are in agreement with other similar electrocatalysts. The results displayed by the complexes in electrochemical OER is suggestive that with efficient tuning of the ligands around the metal centre and the right combination of a conductive material that compliments the gold(I) complexes can be explored in the future as electrocatalysts for OER.

4 | EXPERIMENTAL SECTION

4.1 | General considerations: Synthesis and characterisation

All synthetic experiments were conducted in aerobic conditions using oven dried glassware without dry box, except the preparation of starting materials, aryl triazoles, which were done by employing standard Schlenk technique. Both the aryl triazoles were prepared by a reported method[33] with slight modifications. All chemicals and solvents were procured from commercial sources and used without further purification. Reactions were monitored using thin layer chromatography (TLC) performed on 0.25 mm Merck TLC silica gel plates and UV light was used as a visualising agent. Volatile solvents were removed using rotary evaporator equipped with a dry diaphragm pump (10–15 mmHg) followed by pumping to a constant weight with an oil pump (<300 m Torr). ^{1}H NMR spectra were recorded on Bruker AVANCE III 400 MHz spectrometer and are reported relative to DMSO-d_6 (δ 2.50 ppm). Coupling constants (J) in ^{1}H NMR are reported in Hertz (Hz), and multiplicities are designated as singlet (s), doublet (d), triplet (t), and multiplet (m). Proton-decoupled ^{13}C NMR spectra were recorded at 100 MHz and reported relative to DMSO-d_6 (δ 39.5 ppm). Infrared spectra were recorded on a Bruker ECO-ATR spectrophotometer in the range 600–4000 cm^{-1}. The melting on-sets/points were evaluated by a Stuart Scientific (UK) instrument with an accuracy of ±0.3°C. Elemental analyses were carried out by a Perkin Elmer 2400 Series II CHN/S microanalyser. The electron microscopic images of the complexes were captured using a JEOL JSM-7100F FESEM instrument.

4.2 | Single crystal X-ray crystallography

The crystals were mounted in turn, on a Gemini A Ultra Oxford Diffraction automatic diffractometer equipped with a CCD detector, and used for data collection. X-ray intensity data were collected with graphite monochromated MoKα radiation (λ = 0.71073 Å) at a temperature of 295(2) K, with ω scan mode. Lorentz, polarisation, and empirical absorption correction using spherical harmonics implemented in SCALE3 ABSPACK scaling algorithm (CrysAlis RED, Oxford Diffraction Ltd., Version 1.171.37.46) were applied. All the non-hydrogen atoms were refined anisotropically using full-matrix, least-squares technique. All the hydrogen atoms were found from difference Fourier synthesis after four cycles of anisotropic refinement, and refined as "riding" on the adjacent carbon atom with individual isotropic temperature factor equal 1.2 times the value of equivalent temperature factor of the parent atom. Olex2 and SHELXS programs were used for all the calculations. The geometrical calculations were carried out using the PLATON program. The molecular graphic designs and packing diagram for publication were performed using Olex2 and MERCURY software packages.

4.3 | Synthesis of starting materials

4.3.1 | Synthesis of 4-(2,6 diethylphenyl)-4H-1,2,4-triazole (**2**)

This synthesis involves the methods developed by Holm et al.[33] This is a neat reaction carried out with Schlenk technique. 2,6-Diethyl aniline (11.65 ml, 0.069 M) was added to *N*,*N*-dimethylformamide azine dihydrochloride (15 g, 0.069 M), and the mixture was stirred at 130°C for 72 h. The resulting melt was dissolved in toluene (50 ml), and the solution was basified with 1 M aq. NaOH. The aqueous layer was extracted with toluene (3 × 15 ml). The residue was washed with small amounts of diethyl ether and hexane, and the resulting reddish crude product was purified through column purification to give a light green solid of **2**; Yield: 4.5 g (30%); MP: 150–151°C.

4.3.2 | Synthesis of 4-(2,4,6 trimethylphenyl)-4H-1,2,4 triazole (**3**)

This compound was prepared in an analogous method used for **2**. Here, 2,4,6-mesityl aniline (10.0 mM, 1.35 g) was added to *N*,*N*-dimethylformamide azine dihydrochloride (**3**) (10.0 mM, 2.15 g) under nitrogen atmosphere, and the mixture was stirred at 130°C for 72 h. The resulting melt was dissolved in toluene (50 ml), and the solution was basified with 1 M aq NaOH. The aqueous layer was extracted with toluene (3 × 15 ml). The residue was washed with small amounts of diethyl ether, and the resulting light yellow crude product was purified through column purification to give a colourless solid of **3**; Yield: 1.04 g (56%); M.P.: 233°C.

4.4 | Synthesis of aryl 1,2,4-triazolium salts

4.4.1 | Synthesis of 4-(2,6-diethylphenyl)-1-(pyridin-2-ylmethyl)-4H-1,2,4-triazol-1-ium hexafluorophosphate (**6**)

A solution of 4-(2,6-diethylphenyl)-4H-1,2,4-triazole (**2**) (2.099 mM) in 1,4-dioxane was added a solution of 2-(bromomethyl)pyridine hydrobromide (**1**) (2.099 mM) in 1,4-dioxane. The reaction mixture was stirred for 48 h at 100°C. The reaction mixture resulted in the formation of yellowish brown precipitate after stipulated time, which was filtered under reduced pressure and dried to yield the bromide salt **4** as off-white solid. The bromide salt was translated into its hexafluorophosphate counterpart by the addition of potassium hexafluorophosphate in water methanol mixture (1:9 v/v) at room temperature for 4 h. A white precipitate was obtained, filtered, washed, and dried. Yield: 85%, M.P.: 212-215°C. ^{1}H NMR (400 MHz, DMSO-d_6, 298 K): δ 1.05 (6H, t, CH_3-diethyl phenyl), 2.32 (4H, quart, CH_2-diethyl phenyl), 5.95 (2H, s, CH_2-pyridyl), 7.40 (3H^{Ar}, t, pyridyl), 7.57 (2H^{Ar}, m, phenyl), 7.90 (1H^{Ar}, m, phenyl), 8.48 (1H^{Ar}, d, pyridyl), 9.63 (1H, s, C3-triazole), 10.83 (1H, s, C5-triazole). ^{13}C {^{1}H} NMR (100 MHz, d_6-DMSO, 298 K): δ 15.0 (CH_3-diethyl phenyl), 23.9 (CH_2-diethyl phenyl), 55.6 (N-CH_2 pyridyl), 124.5, 125.2, 127.7 (ArC-pyridyl), 129.5, 132.3, 140.3, 141.0 (ArC-phenyl), 145.8, 146.2 (C3/C5 of triazole), 148.4, 151.0 (ArC-pyridyl). ATR-IR (in cm^{-1}): ~2978 ν(C–H), 1627 ν(C=N, pyridine/triazole), 1085 ν(C–N, pyridine/triazole). Anal. Calcd. for $C_{18}H_{21}F_6N_4P$ (in %): C, 49.3; H, 4.8; N, 12.8. Found: C, 49.8; H, 4.7; N, 13.1.

4.4.2 | Synthesis of 4-mesityl-1-(pyridin-2-ylmethyl)-4H-1,2,4-triazol-1-ium hexafluorophosphate (**7**)

Salt **7** was prepared in manner analogous to that of salt **6**. Yield: 81%. M.P.: 242–243°C. ^{1}H NMR (400 MHz, DMSO-d_6, 298 K): δ 2.09 (6H, s, *o*-CH_3, mesityl), 2.36

(3H, s, *p*-CH_3 mesityl), 5.95 (2H, s, CH_2-pyridyl), 7.22 (2H^{Ar}, br. s, phenyl), 7.47 (1H^{Ar}, br. s, pyridyl), 7.69 (1H^{Ar}, br. s, pyridyl), 7.98 (1H^{Ar}, br. s, pyridyl), 8.57 (1H^{Ar}, br. s, pyridyl), 9.55 (1H, s, C3-triazole), 10.78 (1H, s, C5-triazole). $^{13}C\{^1H\}$ NMR (100 MHz, DMSO-d_6, 298 K): δ 17.6 (*o*-CH_3 mesityl), 21.1 (*p*-CH_2 mesityl), 56.5 (N-CH_2 pyridyl), 123.5, 124.5, 128.5 (ArC-pyridyl), 130.0, 134.9, 138.4, 141.6 (ArC-mesityl), 145.5, 146.0 (C3/C5 triazole), 149.8, 152.3 (ArC-pyridyl). ATR-IR (in cm^{-1}): ~2993 ν(C–H), 1615 ν(C=N, pyridine/triazole), ~1046 ν(C–N, pyridine/triazole).

4.5 | Synthesis of pyridine-functionalized NHC binuclear gold(I) complexes

4.5.1 | Synthesis of binuclear gold(I) complex (**8**)

Salt **5**, 4-(2,6-diethylphenyl)-1-(pyridin-2-ylmethyl)-4H-1,2,4-triazol-1-ium hexafluorophosphate, (0.25 mM) was dissolved in acetonitrile (15 ml) followed by the addition of silver(I) oxide (0.12 mM), and the mixture was stirred at 45°C for 24 h in dark. After which, the reaction mixture was filtered through a celite bed to yield a pale-yellow filtrate. The in situ obtained silver(I) complex solution was converted into gold(I) complex by treating with [AuCl $(SMe)_2$] (0.12 mM) in 15 ml of dichloromethane solution and stirred in room temperature for 4 h in dark. Further, the reaction mixture was passed through a bed of celite to discard silver chloride precipitate, and the filtrate obtained was concentrated to half of its volume under reduced pressure to which was added diethyl ether to yield the gold(I) complex **8** as white solid. Yield: 40.32%. M.P. on-set: 178–182°C. ^1H NMR (400 MHz, DMSO-d_6, 298 K): δ 1.01 (6H, s, CH_3-diethyl phenyl), 2.09 (4H, s, CH_2-diethyl phenyl), 6.39 (2H, s, CH_2-pyridyl), 7.17 (1H^{Ar}, s, pyridyl), 7.41 (2H^{Ar}, br. s, phenyl), 7.59 (1H^{Ar}, br. s, pyridyl), 7.87 (1H^{Ar}, br. s, pyridyl), 8.17 (1H^{Ar}, br. s, phenyl), 8.27 (1H^{Ar}, br. s, pyridyl), 8.45 (1H^{Ar}, br. s, pyridyl), 9.46 (1H, s, C3-triazole). $^{13}C\{^1H\}$ NMR (100 MHz, DMSO-d_6, 298 K): δ 15.0 (CH_3-diethyl phenyl), 24.1 (CH_2-diethyl phenyl), 57.2 (*N*-CH_2 pyridyl), 127.5, 131.2, 132.1 (ArC-pyridyl), 140.7, 140.9, 143.4, 145.9 (ArC-phenyl), 149.9 (C3 triazole), 152.4, 154.5 (ArC-pyridyl), 186.8 (C5 triazole). ATR-IR (in cm^{-1}): ~3054 ν(C–H), 1635 ν(C=N, pyridine/triazole), 1028 ν(C–N, pyridine/triazole). Anal Calcd for $C_{36}H_{40}Au_2F_{12}N_8P_2$ (in %): C, 34.1; H, 3.2; N, 8.8. Found: C, 34.3; H, 3.3; N, 8.8.

4.5.2 | Synthesis of binuclear gold(I) complex (**9**)

Complex **9** was prepared in manner analogous to that of complex **8**, using salt **7**. Yield: 30.43%. M.P. on-set: 184–186°C. ^1H NMR (400 MHz, DMSO-d_6, 298 K): δ 2.09 (6H, s, *o*-CH_3 mesityl), 2.35 (3H, s, *p*-CH_3 mesityl), 6.39 (2H, s, CH_2-pyridyl), 7.00 (1H^{Ar}, br. s, pyridyl), 7.21 (2H^{Ar}, br. s, phenyl), 7.89 (1H^{Ar}, br. s, pyridyl), 8.32 (1H^{Ar}, d, pyridyl), 8.50 (2H^{Ar}, br. s, pyridyl), 9.20 (1H, s, C3-triazole). $^{13}C\{^1H\}$ NMR (100 MHz, DMSO-d_6, 298 K): δ 18.4 (*o*-CH_3 diethyl phenyl), 21.2 (*p*-CH_2 diethyl phenyl), 57.6 (*N*-CH_2 pyridyl), 127.8, 129.5, 130.0 (ArC pyridyl), 130.6, 131.0, 135.0, 140.8 (ArC mesityl), 143.5 (C3 of triazole), 147.3, 153.6 (ArC pyridyl), 168.8 (C5 triazole). ATR-IR (in cm^{-1}): ~3030, 2856 ν(C–H), 1653 ν(C=N, pyridine/triazole), ~1019 ν(C–N, pyridine/triazole).

4.6 | Modified electrode preparation with gold complex–carbon composites

The glassy carbon electrode (GCE) with 3 mm diameter was polished with alumina slurry of assorted sizes, that is, 1.0, 0.3, and 0.05 μm alumina, respectively, and washed with distilled water to obtain a mirror like carbon surface. The electrodes were sonicated in ethanol and water mixture. The gold(I) complexes (0.003 M) with 10 weight % of graphitic mesoporous carbon was dispersed in dichloromethane by sonication for 10 min. Later, 3 μl prepared complex–carbon suspension was drop-casted on the electrode surface and then dried at room temperature overnight.

4.7 | Electrochemical measurements

All electrochemical measurements were carried out using Potentiostat/Galvanostat Model 263A from EG&G Instruments, Princeton Applied Research at room temperature. The electrochemical measurements were carried out in three electrode assembly comprising of SCE (3.5 M KCl) as a reference electrode, platinum wire as a counter electrode, and the gold complex–carbon composite modified GCE as a working electrode in 1 M KOH electrolyte medium. The OER tests were conducted by using linear sweep voltammetry (LSV), the current density was normalised to the geometric surface area of the GCE (0.07 cm^{-2}) and the potential measured versus SCE was converted to reversible hydrogen electrode (RHE) according to the standard Nernst equation.

ACKNOWLEDGEMENTS

NDH thanks the Department of Science and Technology, New Delhi, India, for the financial support through Innovation, Technology Development and Deployment research grant DST/TDT/DDP-33/2018. MA acknowledges the financial support through Researchers Supporting Project number (RSP-2021/147), King Saud University, Riyadh, Saudi Arabia. The support and the instrumentation facilities extended by the Centre for Nano and Material Sciences, Jain University, Bangalore, India, are acknowledged. Authors also thank Raman Research Institute, Bangalore, India, for electrochemical instrumentation facility.

AUTHOR CONTRIBUTIONS

Zhoveta Yhobu: Conceptualization; methodology. **Geetha Basappa Markandeya:** Conceptualization; methodology. **Jan Grzegorz Małecki:** Methodology; validation. **Hosapalya Thimmaiah Srinivasa:** Methodology; validation. **Rangappa S. Keri:** Methodology; software. **Doddahalli Hanumantharayudu Nagaraju:** Supervision. **Mohammad Azam:** Conceptualization. **Saud I. Al-Resayes:** Methodology. **Srinivasa Budagumpi:** Conceptualization; supervision.

DATA AVAILABILITY STATEMENT

Data are available in the article's supporting information.

ORCID

Zhoveta Yhobu https://orcid.org/0000-0003-3401-6783
Geetha Basappa Markandeya https://orcid.org/0000-0003-4445-674X
Jan Grzegorz Małecki https://orcid.org/0000-0001-5571-3196
Hosapalya Thimmaiah Srinivasa https://orcid.org/0000-0002-3940-4868
Rangappa S. Keri https://orcid.org/0000-0001-6262-8379
Doddahalli Hanumantharayudu Nagaraju https://orcid.org/0000-0002-3809-1775
Mohammad Azam https://orcid.org/0000-0002-4274-2796
Saud I. Al-Resayes https://orcid.org/0000-0002-2498-3609
Srinivasa Budagumpi https://orcid.org/0000-0001-6591-7811

REFERENCES

[1] E. Frankland, B. F. Duppa, *J. Chem. Soc.* **1864**, *17*, 29.
[2] W. J. Pope, C. S. Gibson, *J. Chem. Soc., Trans.* **1907**, *91*, 2061.
[3] H. Gilman, L. A. Woods, *J. Am. Chem. Soc.* **1948**, *70*, 550.
[4] G. E. Coates, C. Parkin, *J. Chem. Soc.* **1963**, 421.
[5] W. E. Brenzovich, D. Benitez, A. D. Lackner, H. P. Shunatona, E. Tkatchouk, W. A. Goddard, F. D. Toste, *Angew. Chem. Int. Ed.* **2010**, *49*, 5519.
[6] A. D. Melhado, W. E. Brenzovich, A. D. Lackner, F. D. Toste, *J. Am. Chem. Soc.* **2010**, *132*, 8885.
[7] N. Shapiro, F. Toste, *Synlett* **2010**, *2010*, 675.
[8] A. Arcadi, *Chem. Rev.* **2008**, *108*, 3266.
[9] A. S. K. Hashmi, G. J. Hutchings, *Angew. Chem. Int. Ed.* **2006**, *45*, 7896.
[10] R. Skouta, C. J. Li, *Tetrahedron* **2008**, *64*, 4917.
[11] M. Navarro, *Coord. Chem. Rev.* **2009**, *253*, 1619.
[12] Z. Li, C. Brouwer, C. He, *Chem. Rev.* **2008**, *108*, 3239.
[13] E. Jiménez-Núñez, A. M. Echavarren, *Chem. Rev.* **2008**, *108*, 3326.
[14] N. T. Patil, Y. Yamamoto, *Chem. Rev.* **2008**, *108*, 3395.
[15] A. J. Arduengo, R. L. Harlow, M. Kline, *J. Am. Chem. Soc.* **1991**, *113*, 361.
[16] G. Achar, C. R. Shahini, S. A. Patil, J. G. Małecki, S. Budagumpi, *New J. Chem.* **2019**, *43*, 1216.
[17] M. U. Anu Prathap, C. A. H. Aguilar, T. Pandiyan, R. Srivastava, *J. Appl. Electrochem.* **2013**, *43*, 939.
[18] M. Pažický, A. Loos, M. J. Ferreira, D. Serra, N. Vinokurov, F. Rominger, C. Jäkel, A. S. K. Hashmi, M. Limbach, *Organometallics* **2010**, *29*, 4448.
[19] H. V. Huynh, S. Guo, W. Wu, *Organometallics* **2013**, *32*, 4591.
[20] K. N. Brinda, J. G. Małecki, Z. Yhobu, D. H. Nagaraju, S. Budagumpi, E. S. Erakulan, R. Thapa, *J. Phys. Chem. C* **2021**, *125*, 3793.
[21] Z. Yhobu, K. N. Brinda, G. Achar, J. G. Małecki, R. S. Keri, D. H. Nagaraju, S. Budagumpi, *Appl. Organomet. Chem.* **2021**, *35*, 6446.
[22] Q. Zhang, E. Uchaker, S. L. Candelaria, G. Cao, *Chem. Soc. Rev.* **2013**, *42*, 3127.
[23] H. Zhang, P. K. Shen, *Chem. Rev.* **2012**, *112*, 2780.
[24] X. Zheng, B. Zhang, P. De Luna, Y. Liang, R. Comin, O. Voznyy, L. Han, F. P. García De Arquer, M. Liu, C. T. Dinh, T. Regier, J. J. Dynes, S. He, H. L. Xin, H. Peng, D. Prendergast, X. Du, E. H. Sargent, *Nat. Chem.* **2018**, *10*, 149.
[25] A. Bergmann, E. Martinez-Moreno, D. Teschner, P. Chernev, M. Gliech, J. F. de Araújo, T. Reier, H. Dau, P. Strasser, *Nat. Commun.* **2015**, *6*, 8625.
[26] J. Suntivich, K. J. May, H. A. Gasteiger, J. B. Goodenough, Y. Shao-Horn, *Science (80-.)* **2011**, *334*, 1383.
[27] N. T. Suen, S. F. Hung, Q. Quan, N. Zhang, Y. J. Xu, H. M. Chen, *Chem. Soc. Rev.* **2017**, *46*, 337.
[28] F. Dionigi, P. Strasser, *Adv. Energy Mater.* **2016**, *6*, 1600621.
[29] V. S. Thoi, C. J. Chang, *Chem. Commun.* **2011**, *47*, 6578.
[30] V. S. Thoi, N. Kornienko, C. G. Margarit, P. Yang, C. J. Chang, *J. Am. Chem. Soc.* **2013**, *135*, 14413.
[31] O. R. Luca, D. L. Huang, M. K. Takase, R. H. Crabtree, *New J. Chem.* **2013**, *37*, 3402.
[32] O. R. Luca, J. D. Blakemore, S. J. Konezny, J. M. Praetorius, T. J. Schmeier, G. B. Hunsinger, V. S. Batista, G. W. Brudvig, N. Hazari, R. H. Crabtree, *Inorg. Chem.* **2012**, *51*, 8704.
[33] S. C. Holm, B. F. Straub, *Org. Prep. Proced. Int.* **2011**, *43*, 319.
[34] H. M. J. Wang, I. J. B. Lin, *Organometallics* **1998**, *17*, 972.
[35] S. Guo, J. C. Bernhammer, H. V. Huynh, *Dalton Trans.* **2015**, *44*, 15157.

[36] C. Dash, M. M. Shaikh, R. J. Butcher, P. Ghosh, *Inorg. Chem.* **2010**, *49*, 4972.
[37] H. M. J. Wang, C. S. Vasam, T. Y. R. Tsai, S.-H. Chen, A. H. H. Chang, I. J. B. Lin, *Organometallics* **2005**, *24*, 486.
[38] P. de Frémont, N. M. Scott, E. D. Stevens, S. P. Nolan, *Organometallics* **2005**, *24*, 2411.
[39] J. Turek, Z. Růžičková, E. Tloušťová, H. Mertlíková-Kaiserová, J. Günterová, L. Rulíšek, A. Růžička, *Appl. Organomet. Chem.* **2016**, *30*, 318.
[40] J. C. Bernhammer, H. V. Huynh, *Organometallics* **2014**, *33*, 5845.
[41] T. Simler, K. Möbius, K. Müller, T. J. Feuerstein, M. T. Gamer, S. Lebedkin, M. M. Kappes, P. W. Roesky, *Organometallics* **2019**, *38*, 3649.
[42] F. Song, X. Hu, *Nat. Commun.* **2014**, *5*, 1.
[43] B. S. Yeo, S. L. Klaus, P. N. Ross, R. A. Mathies, A. T. Bell, *ChemPhysChem* **2010**, *11*, 1854.
[44] I. M. Al-Akraa, A. M. Mohammad, M. S. El-Deab, B. E. El-Anadouli, *Arab. J. Chem.* **2017**, *10*, 877.
[45] Y. Matsumoto, S. Yamada, T. Nishida, E. Sato, *J. Electrochem. Soc.* **1980**, *127*, 2360.
[46] P. Rasiyah, A. C. C. Tseung, D. B. Hibbert, *J. Electrochem. Soc.* **1982**, *129*, 1724.
[47] A. C. Ferreira, E. R. Gonzalez, E. A. Ticianelli, L. A. Avaca, B. Matvienko, *J. Appl. Electrochem.* **1988**, *18*, 894.
[48] Y. Gorlin, T. F. Jaramillo, *J. Am. Chem. Soc.* **2010**, *132*, 13612.
[49] H. B. Aiyappa, J. Thote, D. B. Shinde, R. Banerjee, S. Kurungot, *Chem. Mater.* **2016**, *28*, 4375.

SUPPORTING INFORMATION

Additional supporting information can be found online in the Supporting Information section at the end of this article.

How to cite this article: Z. Yhobu, G. B. Markandeya, J. G. Małecki, H. T. Srinivasa, R. S. Keri, D. H. Nagaraju, M. Azam, S. I. Al-Resayes, S. Budagumpi, *Appl Organomet Chem* **2022**, e6837. https://doi.org/10.1002/aoc.6837